

REPORT DOCUMENTATION PAGE

Form Approved
OMB NO. 0704-0188

Public Reporting burden for this collection of information is estimated to average 1 hour per response, including the time for reviewing instructions, searching existing data sources, gathering and maintaining the data needed, and completing and reviewing the collection of information. Send comment regarding this burden estimates or any other aspect of this collection of information, including suggestions for reducing this burden, to Washington Headquarters Services, Directorate for Information Operations and Reports, 1215 Jefferson Davis Highway, Suite 1204, Arlington, VA 22202-4302, and to the Office of Management and Budget, Paperwork Reduction Project (0704-0188), Washington, DC 20503.

1. AGENCY USE ONLY (Leave Blank)		2. REPORT DATE 10/16/2009	3. REPORT TYPE AND DATES COVERED Final Report, 07/01/2003-02/28/2009
4. TITLE AND SUBTITLE MURI Center for Photonic Quantum Information Systems		5. FUNDING NUMBERS DAAD19-03-1-0199	
6. AUTHOR(S) Jelena Vuckovic, Paul Kwiat			
7. PERFORMING ORGANIZATION NAME(S) AND ADDRESS(ES) USA: Stanford University, Uni. Of Illinois at Urbana-Champaign, Harvard University, California Institute of Technology, NIST (Gaithersburg, MD); Canada, University of Toronto; Australia: University of Queensland, Brisbane		8. PERFORMING ORGANIZATION REPORT NUMBER	
9. SPONSORING / MONITORING AGENCY NAME(S) AND ADDRESS(ES) U. S. Army Research Office P.O. Box 12211 Research Triangle Park, NC 27709-2211		10. SPONSORING / MONITORING AGENCY REPORT NUMBER	
11. SUPPLEMENTARY NOTES The views, opinions and/or findings contained in this report are those of the author(s) and should not be construed as an official Department of the Army position, policy or decision, unless so designated by other documentation.			
12 a. DISTRIBUTION / AVAILABILITY STATEMENT Approved for public release; distribution unlimited.		12 b. DISTRIBUTION CODE	
13. ABSTRACT (Maximum 200 words) We have continued the development of several photonic quantum technologies: single-photon and entangled-photon sources from quantum dots and parametric down-conversion; solid-state quantum gates based on quantum dots in semiconductors and on NV centers in diamond; quantum memories using optical storage systems; and high-efficiency single-photon detectors, using optimized visible light photon counters, superconducting bolometers, and frequency upconverters (to be able to detect telecommunication wavelengths using superior visible-wavelength detectors). For most of these devices, we have already successfully performed experimental demonstrations. We have also continued our work on combining these devices into quantum information systems, by continuing to work on and improve the experimental demonstrations of quantum repeater protocols that we, by working on quantum information systems on chip, and of our high-speed quantum cryptography systems, and also by continuing to work on quantum information encoding into transverse spatial modes.			
14. SUBJECT TERMS Quantum information technologies, quantum information systems, single- and entangled photon sources, single and photon number detectors, photon storage, quantum repeater, quantum gates		15. NUMBER OF PAGES 27	16. PRICE CODE
17. SECURITY CLASSIFICATION OR REPORT UNCLASSIFIED	18. SECURITY CLASSIFICATION ON THIS PAGE UNCLASSIFIED	19. SECURITY CLASSIFICATION OF ABSTRACT UNCLASSIFIED	20. LIMITATION OF ABSTRACT U

NSN 7540-01-280-5500

Standard Form 298 (Rev.2-89)
Prescribed by ANSI Std. Z39-18
298-102

Enclosure 1

REPORT DOCUMENTATION PAGE (SF298)
(Continuation Sheet)

Note: 27 pages total

Publications

Submitted to Peer-Reviewed Journals

1. Dirk Englund, Andrei Faraon, Ilya Fushman, and Jelena Vuckovic, "Quantum Dots in Photonic Crystals: From Quantum Information Processing to Single Photon Nonlinear Optics," to appear in special issue of the journal "Photonics and Nanostructures: Fundamentals and Applications (PNFA), (2008).
2. Q. Zhang, H. Takesue, C. Langrock, X. Xie, M. M. Fejer, and Y. Yamamoto, "Hong-Ou-Mandel Dip Using Photon Pairs From a PPLN Waveguide," Submitted to Optics Express (2008).
3. K. Sanaka, A. Pawlis, T. D. Ladd, K. Lischka, and Y. Yamamoto, "Quantum Interference Between Single Photons Emitted by Independent Semiconductor Nanodevices," Submitted to Science (2008).
4. K. Wen, K. Tamaki, and Y. Yamamoto, "Unconditional Security of Single Photon Differential Phase Shift Quantum Key Distribution," Submitted to Phys. Rev. Lett. (2008).
5. D. Press, T. D. Ladd, B. Zhang and Y. Yamamoto, "Complete Quantum Control of a Single Quantum Dot Spin Using Ultrafast Optical Pulses," Submitted to Nature (2008).
6. J. R. Maze, J. M. Taylor, and M. D. Lukin, "Electron Spin Decoherence of Single Nitrogen-Vacancy Defects in Diamond," cond.mat.other/0805.0327, submitted to Phys. Rev. B (2008).
7. M. David Henry and Axel Scherer, "Design Fabrication, and Characterization of a Planar Copper Microcoil for Nuclear Magnetic Resonance Detection" submitted to Proc. IEEE (July 2008).

Published in Peer-Reviewed Journals

1. Andrei Faraon, Ilya Fushman, Dirk Englund, Nick Stoltz, Pierre Petroff, and Jelena Vuckovic, "Coherent Generation of Nonclassical Light on a Chip via Photon-Induced Tunneling and Blockade," to appear in Nature Physics (2008).
2. Andrei Faraon, Ilya Fushman, Dirk Englund, Nick Stoltz, Pierre Petroff, and Jelena Vuckovic, "Dipole Induced Transparency in Waveguide Coupled Photonic Crystal Cavities," Optics Express, Vol 16, pp. 12154-12162 (2008).
3. Ilya Fushman, Dirk Englund, Andrei Faraon, Nick Stoltz, Pierre Petroff, and Jelena Vuckovic, "Controlled Phase Shift With a Single Quantum Dot," Science, Vol. 320, No. 5877, pp. 769-772 (2008).
4. Ilya Fushman, Dirk Englund, Andrei Faraon, and Jelena Vuckovic, "Probing the Interaction Between a Single Quantum Dot and a Photonic Crystal Cavity," Physica Status Solidi (c), Vol. 5, No. 9, 2808-2815 (2008).
5. Andrei Faraon, Dirk Englund, Barry Luther-Davies, Douglas Boulla, Benjamin J. Eggleton, Nick

- Stoltz, Pierre Petroff, and Jelena Vuckovic, "Local Tuning of Photonic Crystal Cavities Using Chalcogenide Glasses," *Appl. Phys. Lett.* Vol. 92, 043123 (Jan 2008).
6. Dirk Englund, Andrei Faraon, Ilya Fushman, Nick Stoltz, Pierre Petroff, and Jelena Vuckovic, "Controlling Cavity Reflectivity With a Single Quantum Dot," *Nature*, Vol. 450, No. 7171, pp. 857-861 (Dec 2007).
 7. Dirk Englund, Hatice Altug, and Jelena Vuckovic, "Low-Threshold Surface-Passivated Photonic Crystal Nanocavity Laser," *Appl. Phys. Lett.*, Vol. 91, 071124 (Aug 2007).
 8. Dirk Englund, Hatice Altug, Ilya Fushman, and Jelena Vuckovic, "Efficient Terahertz Room-Temperature Photonic Crystal Nanocavity Laser," *Appl. Phys. Lett.*, Vol. 91, 071126 (Aug 2007).
 9. Q. Zhang, X. Xie, H. Takesue, S. W. Nam, C. Langrock, M. Fejer, and Y. Yamamoto, "Correlated Photon-Pair Generation in Reverse Proton-Exchange PPLN Waveguides With Integrated Mode Demultiplexer at 10 GHz Clock," *Optics Express* 15, 10288 (Aug 2007).
 10. H. Deng, G. S. Solomon, R. Hey, K. H. Ploog, and Y. Yamamoto, "Spatial Coherence of a Polariton Condensate," *Phys. Rev. Lett.* 99, 126403 (Sep 2007).
 11. Q. Zhang, C. Langrock, H. Takesue, X. Xie, M. M. Fejer, and Y. Yamamoto, "Generation of 10 GHz Clock Sequential Time-Bin Entanglement," *Optics Express* 16, 3293 (Mar 2008).
 12. Q. Zhang, H. Takesue, S. W. Nam, C. Langrock, X. Xie, B. Baek, M. M. Fejer, and Y. Yamamoto, "Distribution of Time-Energy Entanglement Over 100 km Fiber Using Superconducting Single Photon Detectors," *Optics Express* 16, 5776 (Apr 2008).
 13. K. C. Fu, C. Santori, S. M. Clark, C. Stanley, M. C. Holland, and Y. Yamamoto, "Ultrafast Control of Donor-Bound Electron Spins With Single Detuned Optical Pulses," *Nature Physics*, Published online: doi:10.1038/nphys1052 (Aug 2008).
 14. G. Brida, I. Degiovanni, M. Genovese, V. Schettini, S. Polyakov, and A. Migdall, "Experimental Test of Nonclassicality for a Single Particle," *Opt. Express* 16, 11750-11758 (2008).
 15. M. D. Eisaman, E. A. Goldschmidt, J. Chen, J. Fan, and A. Migdall, "Experimental Test of Nonlocal Realism Using a Fiber-Based Source of Polarization-Entangled Photon Pairs," *Phys. Rev. A* 77, 032339 (2008).
 16. J. Chen, J. Fan, M. D. Eisaman, and A. Migdall, "Generation of High-Flux Hyperentangled Photon Pairs Using a Microstructure-Fiber Sagnac Interferometer," *Phys. Rev. A* 77, 053812 (2008).
 17. J. Fan, M. D. Eisaman, and A. Migdall, "Quantum State Tomography of a Fiber-Based Source of Polarization-Entangled Photon Pairs," *Opt. Express* 15, 18339-18344 (2007).
 18. J. Fan, M. D. Eisaman, and A. Migdall, "Bright Phase-Stable Broadband Fiber-Based Source of Polarization-Entangled Photon Pairs," *Phys. Rev. A* 76, 043836 (2007).
 19. V. Schettini, S. V. Polyakov, I. P. Degiovanni, G. Brida, S. Castelletto, and A. L. Migdall, "Implementing a Multiplexed System of Detectors for Higher Photon Counting Rates," *IEEE J. of Selected Topics in Quantum Electronics* 13, 978-983 (2007).
 20. J. Cheung, J. Gardner, A. Migdall, S. Polyakov, and M. Ware, "High Accuracy Dual Lens Transmittance Measurements," *Appl. Opt.* 46, 5396-6403 (2007).
 21. L. Jiang, M. V. Gurudev Dutt, E. Togan, L. Childress, P. Cappellaro, J. M. Taylor, and M. D. Lukin, "Coherence of an Optically Illuminated Single Nuclear Spin Qubit," *Phys. Rev. Lett.* 100, 073001 (2008).

22. L. Jiang, J. Taylor, N. Khaneja, and M. D. Lukin, "Optimal Approach to Quantum Communication Algorithms Using Dynamics Programming," *PNAS*, 104, 17291 (2007).
23. A. V. Akimov, A. Mukherjee, C. L. Yu, D. E. Chang, A. S. Zibrov, P. R. Hemmer, H. Park, and M. D. Lukin, "Efficient Generation of Single Optical Plasmons in Metallic Nanowires Coupled to Quantum Dots." *Nature* 450, 402 (2007).
24. D. E. Chang, A. S. Sorensen, E. Demler, and M. D. Lukin, "A Single-Photon Transistor Using Nanoscale Surface Plasmons," *Nature Physics* 3, 807 (2007).
25. L. Jiang, J. M. Taylor, A. S. Sorensen, and M. D. Lukin, "Distributed Quantum Computation Based on Small Quantum Registers," *Phys. Rev. A* 76, 062323 (2007).
26. J. T. Barreiro, T. -C. Wei, and P. G. Kwiat, "Beating the Channel Capacity Limit for Linear Photonic Superdense Coding," *Nature Physics* 4, 282 (2008).

Papers Published in Non-Peer Reviewed Journals or in Conference Proceedings

1. Dirk Englund, Jelena Vuckovic, "Classical and Quantum Light Sources Based on Photonic Crystals," SPIE Optics and Photonics Meeting, San Diego, Aug. 10-14, 2008 [invited].
2. Jelena Vuckovic, Andrei Faraon, Ilya Fushman, and Dirk Englund, "Controlling Photonic Crystal Cavity Reflectivity With a Single Quantum Dot: From Quantum Information Processing to Single Photon Nonlinear Optics," European Materials Research Society (EMRS) Spring Meeting, Symposium on Active Materials in Photonic Crystals for (Strong) Light Matter Coupling, Strasbourg, France, May 26-30, 2008 [invited].
3. Jelena Vuckovic, Dirk Englund, Andrei Faraon, Ilya Fushman, and Vanessa Sih "Quantum Information Processing With Quantum Dots in Photonic Crystals," SPIE Photonics West Conference, Conference on "Advanced Optical Concepts in Quantum Computing, Memory and Communication," San Jose, CA, Jan. 2008 [invited].
4. Jelena Vuckovic, Dirk Englund, Andrei Faraon, Ilya Fushman, Bryan Ellis, and Hatice Altug "Photonic Crystal Chips for Optical Interconnects and Quantum Information Processing," SPIE Photonics West Conference, Conference on "Photonic Crystal Materials and Devices," San Jose, CA, Jan. 2008 [invited].
5. Jelena Vuckovic, Ilya Fushman, Andrei Faraon, Dirk Englund, Bryan Ellis, Yiyang Gong, and Maria Makarova, "Photonic Crystal Chips for Classical and Quantum Information Processing," ISCS (International Symposium on Compound Semiconductors), Kyoto, Japan, Oct. 15-18, 2007 [invited].
6. Dirk Englund, Andrei Faraon, Ilya Fushman, and Jelena Vuckovic, "Quantum Information Processing on Photonic Crystal Chips," Gordon Conference on Quantum Information, Big Sky Resort, Montana, August 2008 [poster].
7. Andrei Faraon, Ilya Fushman, Dirk Englund, and Jelena Vuckovic, "Quantum Dot-Photonic Crystal Devices for Quantum Information Processing," Gordon Conference on Quantum Information, Big Sky Resort, Montana, August 2008 [poster].

8. Ilya Fushman, Dirk Englund, Andrei Faraon, and Jelena Vuckovic, "Probing a Quantum Dot in the Weak Coupling Regime," CLEO-QELS, San Jose, CA, May 2008.
9. Andrei Faraon, Dirk Englund, Douglas Bulla, Barry Luther-Davies, Benjamin J. Eggleton, Nick Stoltz, Pierre Petroff, and Jelena Vuckovic, "Local Tuning of Photonic Crystal Cavities Using Chalcogenide Glasses," CLEO-QELS, San Jose, CA, May 2008.
10. Dirk Englund, Andrei Faraon, Ilya Fushman, Nick Stoltz, Pierre Petroff, and Jelena Vuckovic, "Coherent Probing and Saturation of a Strongly Coupled Quantum Dot," CLEO-QELS, San Jose, CA (May 2008).
11. Dirk Englund, Andrei Faraon, Ilya Fushman, and Jelena Vuckovic, "Controlling Cavity Reflectivity With a Single Quantum Dot," Frontiers in Optics – Laser Science, San Jose, CA – postdeadline paper (2007).
12. Dirk Englund, Ilya Fushman, Jelena Vuckovic, and Hatice Altug, "Terahertz Modulation Room-Temperature Photonic Crystal Nanocavity Laser," Frontiers in Optics – Laser Science, San Jose, CA (2007) [paper FTuT3].
13. S. V. Polyakov, V. Schettini, I. P. Degiovanni, G. Brida, and A. Migdall, "Multiplexed Photon-Counting Detectors," Proc. SPIE 6900, 690019 (2008).

Papers Presented at Meetings, But Not Published in Conference Proceedings

1. Ilya Fushman and Jelena Vuckovic, "Quantum Dots in Photonic Crystals: From Quantum Information Processing to Single Photon Nonlinear Optics," Quantum Cairns International Workshop, Palm Cove, Cairns, Australia (June 30-July 3, 2008).
2. Dirk Englund and Jelena Vuckovic, "Classical and Quantum Information Processing With Quantum Dots in Photonic Crystals," CIPS Annual Meeting, Nanophotonics Session, MIT, Cambridge, MA (May 2008).
3. Andrei Faraon and Jelena Vuckovic, "Classical and Quantum Information Processing Using Photonic Crystals," Annual Meeting of CUDOS (Centre for Ultrahigh-bandwidth Devices for Optical Systems, an ARC Centre of Excellence), Sydney, Australia (February 2008).
4. Jelena Vuckovic, Dirk Englund, Andrei Faraon, and Ilya Fushman, "Quantum Information Processing With Quantum Dots in Photonic Crystals," Stanford Photonics Research Center Annual Meeting, Stanford University (September 2007).
5. Jelena Vuckovic, "Quantum Dots in Photonic Crystals: From Quantum Information Processing to Single Photon Nonlinear Optics," Stanford University, Ginzton Lab Seminar (April 2008).
6. Y. Yamamoto, "Quantum Information Systems Based on Electron Spins Controlled by Coherent Optical Pulses," The 10th Asia Pacific Physics Conference, Pohang, Korea (August 24, 2007).
7. Y. Yamamoto, "Quantum Communication, Computation and Simulation Based on Semiconductor Cavity QED Systems," QuAMP 2007, London, UK (September 13, 2007).

8. T. D. Ladd, "High Speed Quantum Repeaters and Computers Based on Semiconductor Cavity QED," Quantum Computing Workshop, Princeton, NJ (September 20, 2007).
9. Y. Yamamoto, "Photonic Quantum Information Systems," MURI Center for Photonic Quantum Information Systems Annual Meeting, Stanford, CA (October 3, 2007).
10. K. Sanaka, A. Pawlis, T. D. Ladd, and Y. Yamamoto, "Quantum-Welled 19F:ZnSe Microdisk for Cavity Quantum Electrodynamics," MURI Center for Photonic Quantum Information Systems Annual Meeting, Stanford, CA (October 3, 2007).
11. T. D. Ladd, R. Van Meter, A. Fowler, W. J. Munro, K. Nemoto, and Y. Yamamoto, "Quantum Computer Architecture Based on Semiconductor Microphotonics," MURI Center for Photonic Quantum Information Systems Annual Meeting, Stanford, CA (October 3, 2007).
12. H. Takesue, S. W. Nam, Q. Zhang, R. Hadfield, T. Honjo, K. Tamaki, and Y. Yamamoto, "Progress in Differential Phase Shifted (DPS) Quantum Key Distribution," MURI Center for Photonic Quantum Information Systems Annual Meeting, Stanford, CA (October 3, 2007).
13. Q. Zhang, C. Langrock, H. Takesue, X. Xie, Y. Yamamoto, and M. M. Fejer, "Generation and Detection of C-Band Entangled Photon Pairs at a 10 GHz Clock Rate," MURI Center for Photonic Quantum Information Systems Annual Meeting, Stanford, CA (October 3, 2007).
14. S. Clark, K. Fu, T. Ladd, C. Santori, C. Stanley, M. C. Holland, and Y. Yamamoto, "Ultrafast Control of Electron Spins Bound to Neutral Donors for Quantum Information Processing," MURI Center for Photonic Quantum Information Systems Annual Meeting, Stanford, CA (October 3, 2007).
15. S. Clark, K. Fu, T. Ladd, C. Santori, C. Stanley, M. C. Holland, and Y. Yamamoto, "Ultrafast Control of Electron Spins Bound to Neutral Donors for Quantum Information Processing," CIS Advisory Committee Meeting, Stanford, CA (November 14, 2007).
16. Y. Yamamoto, "Quantum Information System for Which Light is Used," The 17th Quantum Information Technology Symposium, Okayama, Japan (November 23, 2007).
17. T. D. Ladd, R. van Meter (Keio/NII), A. Fowler, B. Munro, K. Nemoto, and Y. Yamamoto, "Toward Fault-Tolerance in a Quantum Computer Architecture Based on Semiconductor Microphotonics," The First International Conference on Quantum Error Correction, QEC 07, Los Angeles, CA (December 20, 2007).
18. K. Wen, K. Tamaki, H. Takesue, S. W. Nam, Q. Zhang, R. Hadfield, T. Honjo, C. Langrock, M. M. Fejer, and Y. Yamamoto, "Unconditional Security of Differential Phase Shift Quantum Key Distribution With Single Photon Source," SPRC Quantum Technologies Workshop, Stanford, CA (April 19, 2008).
19. D. Sleiter, T. Horikiri, K. Nozawa, T. Ladd, K. De Greve, Q. Zhang, N. Y. Kim, M. Notomi, and Y. Yamamoto, "Optical Interface to Silicon-Based Nuclear-Spin Quantum Memory," SPRC Quantum Technologies Workshop, Stanford, CA (April 19, 2008).
20. S. Koseki, K. De Greve, B. Zhang, and Y. Yamamoto, "Monolithic Waveguide-Coupled GaAs Microdisks With InGaAs Quantum Dots," SPRC Quantum Technologies Workshop, Stanford, CA (April 19, 2008).
21. T. D. Ladd, R. Van Meter, A. G. Fowler, W. J. Munro, K. Nemoto, and Y. Yamamoto, "Quantum Computer Architecture Based on Semiconductor Microphotonics," SPRC Quantum Technologies Workshop, Stanford, CA (April 19, 2008).

22. S. Clark, K. Fu, T. D. Ladd, C. Santori, C. Stanley, M. C. Holland, and Y. Yamamoto, "Ultrafast Control of Electron Spins Bound to Neutral Donors for Quantum Information Processing," SPRC Quantum Technologies Workshop, Stanford, CA (April 19, 2008).
23. D. Press, S. Goetzinger, Y. Yamamoto, S. Reitzenstein, and A. Forchel, "Photon Antibunching From a Strongly-Coupled QD-Microcavity System," SPRC Quantum Technologies Workshop, Stanford, CA (April 19, 2008).
24. Q. Zhang, H. Takesue, C. Langrock, X. Xie, M. M. Fejer, and Y. Yamamoto, "Hong-Ou-Mandel Dip by Photon Pair From PPLN Waveguide," CLEO/QELS 08, QFE1, San Jose, CA (May 9, 2008).
25. J. T. Barreiro and P. G. Kwiat, "Hyperentanglement-Assisted Dense Coding: Beating the Channel-Capacity 'Limit'," American Phys. Soc. March Meeting, New Orleans, LA (Mar. 10-14, 2008).
26. S. Jobling, K. McCusker, and P. G. Kwiat, "Adaptive Optics for Improved Mode-Coupling Efficiencies," presented at CLEO/QELS, San Jose, CA (May 4-9, 2008).
27. K. T. McCusker, N. A. Peters, A. P. VanDevender and P. G. Kwiat, "A Deterministic Single-Photon Source," presented at CLEO/QELS, San Jose, CA (May 4-9, 2008).
28. P. G. Kwiat and J. T. Barreiro, "Hyperentanglement-Enhanced Quantum Information," Quantum Information and Control, Cairns, Queensland, Australia (June 30-July 3, 2008).
29. R. Rangarajan, "Developing Enabling Technologies for Optical Quantum Information: Detectors & Sources," 4th Asia Pacific Conference in Quantum Information Science, Cairns, Queensland, Australia (July 2-5, 2008).
30. R. Rangarajan, "High-Efficiency Photon-Number-Resolving Detectors," 21st Congress of the International Commission for Optics (ICO), Sydney, Australia (July 7-10, 2008).

Report of Inventions

1. Faraon, I. Fushman, D. Englund, and J. Vuckovic, "Optical Cavity Emitter Arrangements With Spectrally-Aligned Quantum Dots And Methods Therefor," Stanford Disclosure S07-078 (US patent filed, June 6, 2008, Serial No. s12/134,414).
2. E. Waks and J. Vuckovic, "Dipole Induced Transparency in Photonic Crystal Cavity-Waveguide System," Stanford Disclosure S05-380 (US patent filed, Oct. 2007, Serial No. 11/977,244)
3. Alan Migdall, "FPGA-Based Multicoincidence Time Stamping Board," US patent application process begun.

Scientific Personnel Supported by This Project

Senior Researchers

1. Jelena Vuckovic, Stanford
2. Alan Migdall, NIST
3. Mikhail Lukin, Harvard
4. Martin M. Fejer, Stanford
5. Daniel F. V. James, Univ. Toronto
6. Paul Kwiat, UIUC
7. Axel Scherer, Caltech
8. James Eckstein, UIUC
9. Yoshihisa Yamamoto, Stanford

Postdoctoral Scholars

1. Vanessa Sih, Stanford/Vuckovic

Graduate Students

1. Dirk Englund, Stanford/Vuckovic (on NSF Fellowship, except summer)
2. Andrei Faraon, Stanford/Vuckovic
3. Ilya Fushman, Stanford/Vuckovic (on NDSEG Fellowship, except summer)
4. David Press, Stanford/Yamamoto
5. Neil Na, Stanford/Yamamoto
6. Emre Togan, Harvard/Lukin
7. Radhika Rangarajan, UIUC
8. Kevin McCusker, UIUC
9. Uday Khankhoje, CalTech/Scherer
10. Kevin Inderhees, UIUC
11. Tim McArdle, UIUC

Research Scientists

1. Michael Goggin (sabbatical Professor from Truman State University), UIUC
2. Roger Route, Stanford/Fejer
3. Carsten Langrock, Stanford/Fejer

Undergraduate Students

1. Matthew Mahowald (UIUC)
2. Dickson Thain (UIUC)

Administrative Staff

1. Ingrid Tarien, Stanford (admin associate to the PI)

Scientific Personnel Supported by Other Sources, But Working on the Project (e.g., funded internally by a laboratory, or by a fellowship)

Senior Researchers

Postdoctoral Scholars

1. Kaoru Sanaka, Stanford/Yamamoto

2. Thaddeus Ladd, Stanford/Yamamoto
3. Qiang Zhang, Stanford/Yamamoto
4. Tomoyuki Horikiri, Stanford/Yamamoto
5. Gurudev Dutt, Harvard/Lukin
6. Frank Koppens, Harvard/Lukin
7. Philip Walther, Harvard/Lukin
8. Jun Chen, NIST/Migdall
9. Aaron Pearlman, NIST/Migdall

Graduate Students

1. Yiyang Gong, Stanford/Vuckovic (on NDSEG Fellowship)
2. Arka Majumdar, Stanford/Vuckovic (on SGF Fellowship)
3. Kristiaan De Greve, Stanford/Yamamoto
4. Darin Sleiter, Stanford/Yamamoto
5. Shinichi Koseki, Stanford/Yamamoto
6. Susan Clark, Stanford/Yamamoto
7. Kai Wein, Stanford/Yamamoto
8. Michal Bajesy, Harvard/Lukin
9. Darrick Chang, Harvard/Lukin
10. Yiwen Chu, Harvard/Lukin
11. Alexi Gorshkov, Harvard/Lukin
12. Liang Jiang, Harvard/Lukin
13. Jeronimo Maze, Harvard/Lukin
14. Aryesh Mukherjee, Harvard/Lukin
15. Brendan Shields, Harvard/Lukin
16. Julio Barreiro, UIUC
17. Elizabeth Goldschmidt, NIST/Migdall
18. Sandra Cremer, NIST/Migdall
19. Jason Pelc, Stanford/Fejer

Research Scientists

1. Jingyung Fan, NIST/Migdall
2. Sergey Polyakov, NIST/Migdall
3. Bingyang Zhang, Stanford/Yamamoto
4. Alexander Zibrov, Harvard/Lukin
5. Alexey Akimov, Harvard/Lukin
6. Alexey Trifonov, Harvard/Lukin

Undgraduate Students

1. Stephen Altamirano, Stanford/Vuckovic (supported from the Physics Summer Research program)
2. Asmita Kumar, Stanford/Vuckovic (supported by Research Experience for Undergraduates)
3. Alex Hegyi, Stanford/Yamamoto
4. Darcy Barron, UIUC
5. Joseph Gibney, Harvard/Lukin

Administrative Staff

1. Yurika Peterman, Stanford/Yamamoto
2. Rieko Sasaki, Stanford/Yamamoto

Scientific progress and accomplishments

1. Photon sources and quantum gates

We are pursuing several materials systems for solid-state implementation of nonclassical light sources (high-efficiency and high-indistinguishability single-photon sources and entangled-photon sources) and of quantum gates: InAs quantum dots in photonic crystals (Vuckovic), InAs quantum dots in micropost microcavities and semiconductor impurities (Yamamoto), NV centers in diamond (Lukin), parametric down-conversion in bulk and waveguide geometries (Kwiat and Fejer), and microstructure fiber-based systems (Migdall).

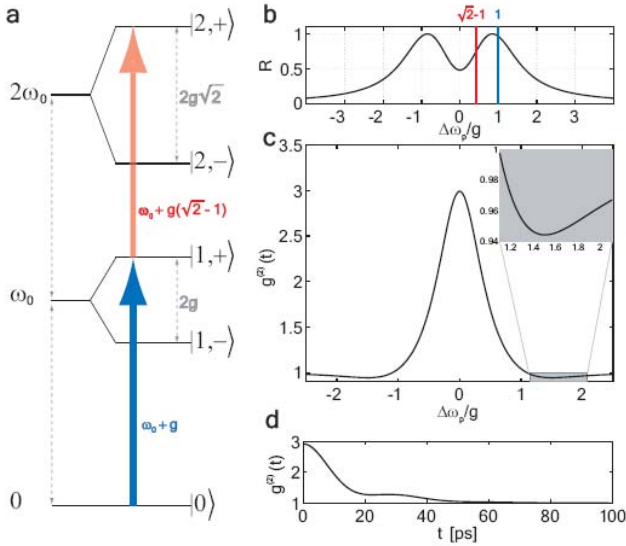
Quantum information processing with quantum dots in photonic crystals (Vuckovic)

The platform we use in our experiments is InAs quantum dots (QD) embedded in GaAs photonic crystal circuits. The quantum dot material is grown by our collaborators at UCSB (Pierre Petroff) and photonic crystals are fabricated by our group in the Stanford Nanofabrication Facility (SNF). Our experimental Q-factors exceed 25000 for the cavities with mode volumes below $V \sim (\lambda/n)^3$ (which is state of the art Q/V for GaAs QDs and operating wavelength around 900 nm).

In order to make use of cavity QED effects for quantum information processing, the quantum dot needs to be addressed coherently. We have probed the QD-cavity-coupled system coherently, in reflectivity, for the first time in solid state [Englund et al, Nature, 2007]. As expected, a dip in reflectivity occurs for the strongly coupled system, and the experimental results show an excellent match with theory. At higher intensities of the probe beam, we observe rapid saturation of the transmission dip. The saturation power inside the cavity is 20nW, corresponding to an average photon number inside the cavity of $\langle n_{\text{cav}} \rangle \sim 0.5$ in agreement with previous predictions for giant optical nonlinearity in a microcavity.

When the cavity is not coupled to a QD, it is possible to inject external photons right at the cavity resonance. In contrast, when a strongly coupled quantum dot interacts with the cavity and is resonant with it, injecting a photon at the cavity resonance is not possible, as shown in Figs. 1. From a quantum mechanical point of view, there is no allowed energy state at that frequency, because the eigenstates of the cavity-QD system no longer correspond to those of the QD and the cavity, but become mixed. In other words, in the strong coupling regime of cavity QED, the quantum dot and the cavity cannot be treated anymore as distinct entities: entangled modes of the dot and the cavity field are formed (we refer to these states as “dressed states” - see Fig. 1). The energy of the n-th dressed states is given by $n\hbar\omega_0 \pm g\sqrt{n+1}$, where n is the number of photons injected into the cavity and ω_0 is the cold cavity mode frequency. The $2g\sqrt{n+1}$ splitting occurs due to the coherent exchange between n and n+1 photons in the cavity, mediated by the QD. In the time domain the system oscillates at a frequency $2g\sqrt{n+1}$ between the state of an excited quantum dot and n photons in the cavity, and quantum dot in the ground state and n+1 photon in the cavity.

With the strongly coupled QD-cavity system, consider the case where a photon is not injected exactly at the cavity resonance ω_0 but at a frequency corresponding to one of the first two dressed states ($\omega_0 \pm g$) (see Fig. 1). In this case the photon can couple to the cavity. If the second photon with the same frequency as the first one is sent toward the cavity, it can no longer be coupled because there is no allowed transition with that energy. Therefore, in the strong coupling regime, the system cannot absorb two photons with the same frequency one immediately after the other; this is an effect known as the *photon blockade*. This effect is a result of the fact that the ladder of the dressed states is anharmonic, as shown in Fig. 1. This effect has so far been demonstrated only in atomic physics system, and we recently demonstrated it in solid state [Faraon et al., Nature Physics, in press, 2008].



delays greater than ~ 5 ps, corresponding to the cavity photon lifetime.

Fig. 1: (a) Energy diagram showing the energy levels of the strongly coupled cavity/QD system. The energy difference between consecutive levels is not constant as shown by the blue and the red arrows. This anharmonic spacing of the levels causes phenomena such as photon blockade and photon bunching (photon induced tunneling). (b) Simulated output intensity for a probe frequency tuned through the cavity/QD strongly coupled system. The red and blue lines indicate the transitions $|0\rangle \rightarrow |1,+\rangle$ and $|1,+\rangle \rightarrow |2,+\rangle$. Photon blockade is expected at detuning of the probe frequency from the bare cavity frequency equal to $\Delta\omega_p/g \sim 1$ because the absorption of a photon into $|1,+\rangle$ suppresses the probability of absorbing a second photon of the same energy for a transition to $|2,+\rangle$. As $\Delta\omega_p \rightarrow 0$ the absorption of a photon into the first dressed state (polariton) enhances the absorption probability into higher order polaritons. (c) Computed second-order correlation $g^{(2)}(0)$ for a coherent laser probe reflected from the cavity. Inset shows that photon blockade ($g^{(2)} < 1$) is expected when the probe detuning is $\Delta\omega_p/g \sim 1.5$ (and not $\Delta\omega_p/g \sim 1$) because of the finite linewidth of the polaritons. As $\Delta\omega_p \rightarrow 0$ the output field is bunched (i.e., $g^{(2)} > 1$). (d) Simulated time dependence of the second-order correlation for $\Delta\omega_p = 0$. The value for $(g^{(2)}(\tau))$ drops rapidly for time

Another effect that we recently observed in the same system is *photon-induced tunneling* – never previously expected in any other system, including atomic physics. This effect is expected when the probe frequency is near the bare cavity resonance ($\omega_p - \omega_0 = \Delta\omega_p \rightarrow 0$): the absorption of a first photon enhances the absorption of subsequent photons so the output consists of “photon bunches.” In Fig. 1(b) we show the output spectrum as the probe is tuned through the cavity and mark the resonance of the transitions $|0\rangle \rightarrow |1,+\rangle$ and $|1,+\rangle \rightarrow |2,+\rangle$. As $\Delta\omega_p \rightarrow 0$, the probability of absorbing the first photon decreases. However, if a photon is nevertheless absorbed, it enhances the probability of capturing the second photon. This process produces a photon-bunched output. The expected second-order photon correlation function for our system is shown in Fig. 1(c), where we plot the dependence of $g^{(2)}(0)$ for different detuning $\Delta\omega_p$ of the probe from the bare cavity frequency ω_0 . As expected from the intuitive argument above, the simulation predicts photon bunching as $\Delta\omega_p \rightarrow 0$, i.e., $g^{(2)} > 1$. Photon blockade (i.e., $g^{(2)} < 1$) is evident in the antibunched region near $\Delta\omega_p \sim \pm 1.5g$ (see inset of Fig. 1(c)), as a result of the described photon blockade. The blockade does not occur for $\Delta\omega_p = \pm g$ as previously explained, but at $\Delta\omega_p \sim \pm 1.5g$, because the linewidth of the eigenstates ($\sim \kappa$) is comparable to the polariton splitting ($\sim 2g$).

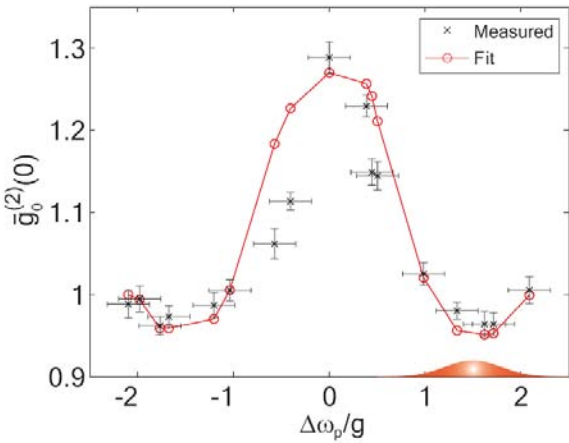


Fig. 2: Measured second-order correlation function $g^{(2)}(0)$ for different detunings between the probe and the bare cavity frequency, $\Delta\omega_p$. As the probe is tuned through the resonance of the QD-cavity system, the output field shows antibunched and bunched behavior as it transitions from photon blockade regime to photon-induced tunneling regime.

As shown in Fig. 2, we have recently experimentally demonstrated this theoretical prediction in a QD-PC cavity system [Faraon et al., Nature Physics, 2008]. Thus, the probability of transmitting a specific number of photons can be tailored by controlling detuning between the probe beam and the bare cavity frequency $\Delta\omega_p$.

This can be employed to generate nonclassical states of light on a chip (by reflecting a coherent beam from a cavity QED system), which is also of interest for quantum information processing.

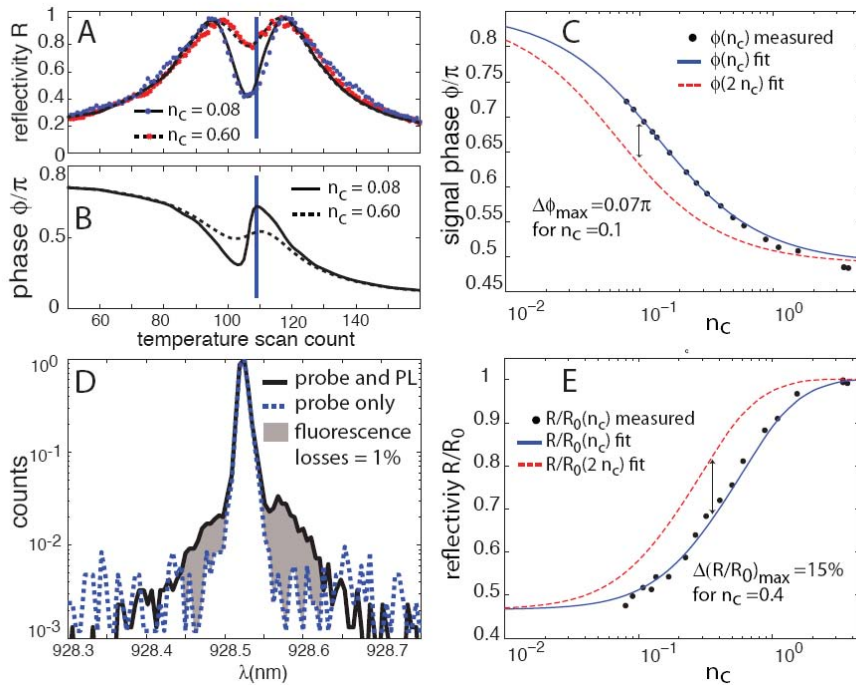


Fig. 3. Nonlinear response of the QD-PC cavity system to single-wavelength excitation with near saturation at control photon number $n_c=0.6$ (A,B). Each temperature scan count corresponds to a particular detuning between the cavity and QD. At a detuning of 0.014 nm ($g/3.5$) from the dot resonance (vertical line in B), the phase changes by 0.24π when intracavity control photon number n_c increases from 0.08 to 3 (C). The phases derived from experimental scans (points) agree with theory (solid line). The dashed red curve is the fit to experimental results evaluated at control powers of $2n_c$. The signal phase shift due to the doubled signal photon number $\phi(n_c) - \phi(2n_c)$ is maximized at $n_c=0.1$ (arrow). (D) The main loss mechanism due to fluorescence from the quantum dot corresponds to $\sim 1\%$ photon loss. (E) Reflectivity power dependence. Points correspond to experimental data for reflectivity (R) normalized by the calculated value of reflectivity from a cavity with no QD (R_0).

We have also recently shown that a single quantum dot (QD) coupled to a photonic crystal(PC) nanocavity can facilitate controlled phase and amplitude modulation between two modes of light at the single photon level, which is crucial for implementation of controlled phase gates [Fushman et al, Science, 2008]. We have observed phase shifts up to $\pi/4$ and amplitude modulation up to 50%. This is accomplished by varying the photon number in the control beam at the wavelength which is the same as the signal, or at a wavelength which is detuned by several QD linewidths from the signal. The results are shown in Fig. 3. Until our demonstration, the largest nonlinearities have been realized with single atoms and atomic ensembles.

Single electron spin manipulation in solid-state (Yamamoto)

We have experimentally demonstrated ultra-fast single electron spin manipulation (a one-qubit gate) using off-resonant optical Raman pulses of picosecond duration. The two experimental systems are an ensemble of neutral donor electrons in a bulk GaAs crystal, and a single electron trapped in an isolated InGaAs quantum dot embedded in GaAs matrix under a dc magnetic field. The electron spin Zeeman sub-level couple to the lowest energy bound exciton state via self-chosen upper and lower side bands of the control optical pulses, as shown in Fig. 4 (a)-(c). An experimental setup for initial optical pumping, optical-pulse-controlled spin manipulation and final optical detection is shown in Fig. 4 (d). As shown in Fig. 5(a), we could observe coherent Rabi oscillations up to integrated pulse area of 12π . The fidelities for a $\pi/2$ -pulse and π -pulse are 93% and 89%, respectively. By using two $\pi/2$ -pulses, separated a varying time τ , we constructed a Ramsey interferometer for an electron spin and observed high visibility, as shown in Fig. 5(b). Such ultra-fast control of a single electron spin is a useful tool for future quantum repeaters and quantum computers.

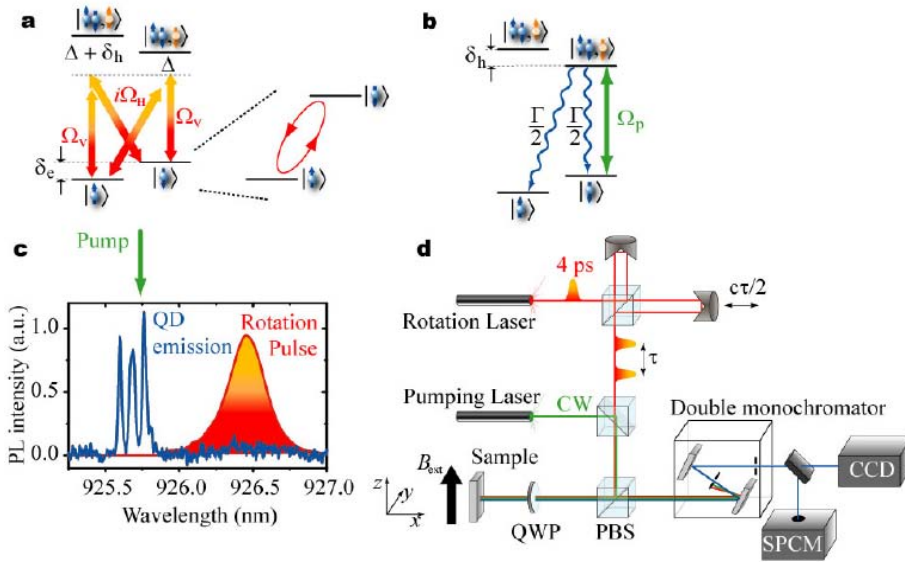


Fig. 4. Experimental methods to initialize, control, and measure a single electron spin. **a**, The spin rotation scheme involves a stimulated Raman transition via two independent Λ -systems. The 4-level system is effectively reduced to a 2-level system if the Rabi frequencies $\Omega_{H,V}$ are much larger than the detuning Δ . **b**, The spin initialization and measurement scheme performed by optical pumping. **c**, Measured photoluminescence spectrum of the charged QD excited by an above-bandgap 785 nm laser. The rotation pulse detuned by $\Delta = 290$ GHz below the lowest transition. **d**, Experimental setup. One or two rotation pulses may be sent to the sample during each experimental cycle, to observe Rabi oscillations or Ramsey

interference, respectively. The time delay τ between pairs of pulses is controlled by a retroreflector mounted on a computer-controlled translation stage. QWP: quarter wave plate, PBS: polarizing beamsplitter.

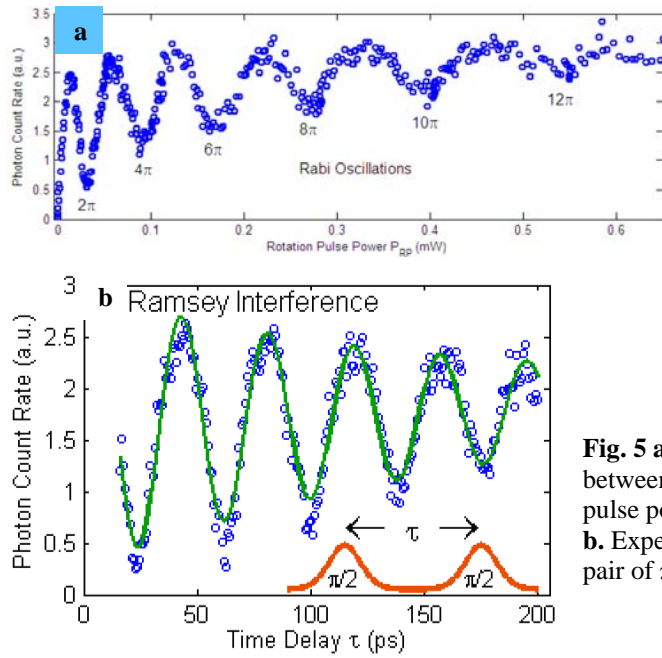


Fig. 5 a. Experimental demonstration of Rabi oscillations. Rabi oscillations between the spin states are evident in the oscillating photon signal as rotation pulse power P_{RP} is increased. **b.** Experimental demonstration of Ramsey fringes. Ramsey interference for a pair of $\pi/2$ pulses, showing photon count rate versus time delay between pulses.

Impurity-based single-photon sources (Yamamoto)

We have also demonstrated the generation of indistinguishable single photons from two identical single-photon emitters: ^{19}F donor impurities in ZnSe quantum well. Quantum indistinguishability was confirmed by observation of a Hong-Ou-Mandel dip.

Plasmonic nanostructures for quantum info processing (Lukin)

Control over the interaction between single photons and individual optical emitters is an outstanding problem in quantum science and engineering. It is of interest for ultimate control over light quanta, as well as for potential applications such as efficient photon collection, single-photon switching and transistors, and long-range optical coupling of quantum bits. Recently, substantial advances have been made towards these goals, based on modifying photon fields around an emitter using high-finesse optical cavities. We demonstrated a cavity-free, broadband approach for engineering photon-emitter interactions via sub-wavelength confinement of optical fields near metallic nanostructures. When a single CdSe quantum dot is optically excited in close proximity to a silver nanowire, emission from the quantum dot couples directly to guided surface plasmons in

the nanowire, causing the wire's ends to light up. Non-classical photon correlations between the emission from the quantum dot and the ends of the nanowire demonstrate that the latter stems from the generation of single, quantized plasmons. Results from a large number of devices show that efficient coupling is accompanied by more than 2.5-fold enhancement of the quantum dot spontaneous emission, in good agreement with theoretical predictions. [Nature, 450, 402 (2007)].

Photons rarely interact—which makes it challenging to build all-optical devices in which one light signal controls another. Even in nonlinear optical media, in which two beams can interact because of their influence on the medium's refractive index, this interaction is weak at low light levels. We proposed a novel approach to realizing strong nonlinear interactions at the single-photon level, by exploiting the strong coupling between individual optical emitters and propagating surface plasmons confined to a conducting nanowire. We showed that this system can act as a nonlinear two-photon switch for incident photons propagating along the nanowire, which can be coherently controlled using conventional quantum-optical techniques. Furthermore, we discuss how the interaction can be tailored to create a single-photon transistor, where the presence (or absence) of a single incident photon in a 'gate' field is sufficient to allow (or prevent) the propagation of subsequent 'signal' photons along the wire [Nature Physics 3, 807 (2007)].

A bright single-mode waveguide-based parametric down-conversion (PDC) source (Fejer, Yamamoto)

The Fejer group is developing integrated devices for quantum optics applications based on nonlinear optical processes in reverse-proton-exchanged (RPE) periodically poled lithium niobate (PPLN) waveguides. During the last year, researchers in Fejer's and Yamamoto's groups have been conducting system experiments using waveguide-based up- and down-conversion devices to demonstrate a wide variety of applications such as high-speed time-bin entanglement and long-distance entanglement distribution as well as quantum optical effects (Hong-Ou-Mandel dip).

In particular, we succeeded in implementing a 10-ps correlated photon pair generator in RPE PPLN waveguides using integrated mode demultiplexers at a wavelength of 1.5 μm and a clock of 10 GHz [Zhang et al., Optics Express, 2007] as shown in Fig. 6. In this experiment, we used superconducting single-photon detectors due to their superior performance with respect to timing jitter as compared to the silicon-based single-photon-counting modules used in the previously reported upconversion-based detectors [Langrock et al., Optics Letters, 2005]. We observed a coincidence-to-accidental count ratio (CAR) as high as 4000 (see Fig. 7), which should make this source useful for applications in quantum information systems as well as quantum entanglement experiments.

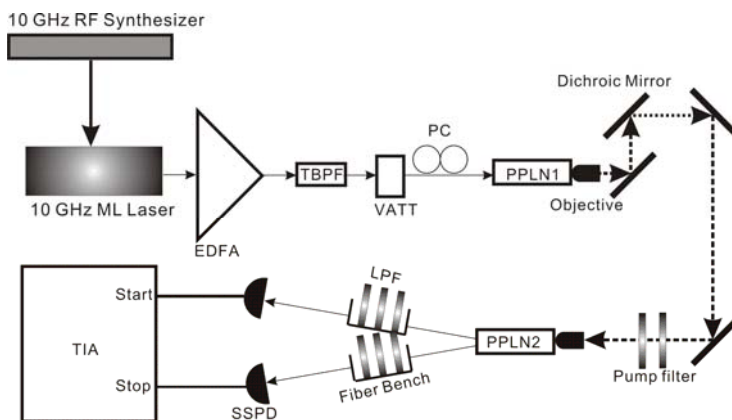


Fig. 6. Diagram of the experimental setup. TBPF: tunable band-pass filter. VATT: variable fiber attenuator. PPLN1: a periodically poled lithium niobate waveguide for second harmonic generation of the pump source. Pump filter: 780 nm bandpass filter to remove 1.5- μm background. PPLN2: a fiber pigtailed asymmetric Y-junction periodically poled lithium niobate waveguide for parametric down-conversion. LPF: long-pass filter to remove the residual pump light. SSPD: superconducting single-photon detector. TIA: time interval analyzer. Solid lines represent fiber and dotted lines represent free-space propagation.

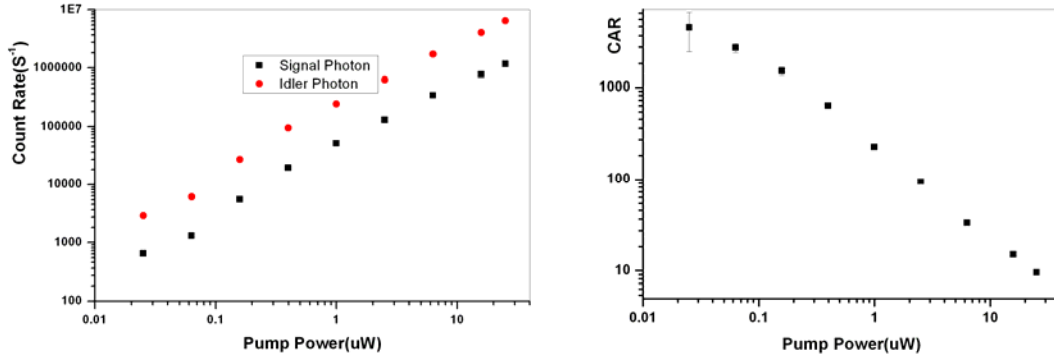


Fig. 7. (left) Single-photon count rates from two superconducting single-photon detectors respectively detecting the two photons in a correlated pair. Black squares represent signal photon and red circles idler photons. The difference in count rates at any given pump power is mainly due to different quantum efficiency of the two SSPDs in our experiment. (right) CAR of the correlated photon pair generation. The x-axis is the 781.5nm pump power generated by the first SH chip. All data points are taken with a 5×10^8 start signal pass except for the one with highest CAR, where we only took 5×10^7 signal instead due to the low count rate. This is also the main reason of its large error bar.

With only minor modifications to the experimental setup described above (one fiber-based 10-GHz Mach-Zehnder interferometer was installed into each arm of the output of the PPLN-based down-converter), we then demonstrated telecom-band sequential time-bin entangled photon-pair generation at a repetition rate of 10 GHz [Zhang et al., Optics Express, March 2008]. Here, we used the above-mentioned upconversion-based single-photon detectors and were able to observe an entangled-photon-pair flux of 313 Hz and a two-photon-interference-fringe visibility of 85.32% (see Fig. 8) without subtraction of accidental noise contributions.

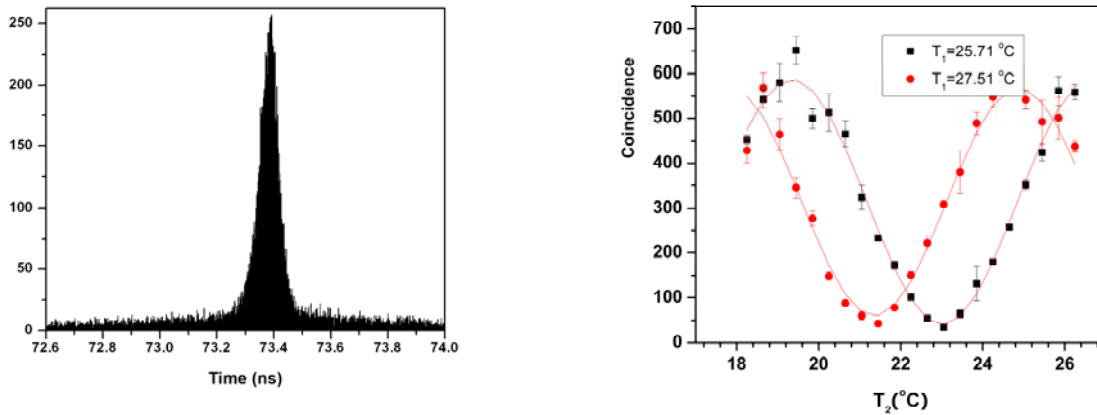


Fig. 8. (left) Histogram of the time spectrum of the correlated photon pairs. (right) Coincidence interference fringes observed in the experiment. T1 and T2 are the temperatures of the Mach-Zehnder interferometers in the signal and idler channels, respectively. All coincidence points in the figure are derived from one million start triggers for the TIA.

The logical next step was to try to propagate time-energy entangled photons through a 100-km-long spool of dispersion-shifted telecommunication fiber to demonstrate entanglement distribution. In the experiment, we used the above described asymmetric Y-junction RPE PPLN waveguide to generate the time-energy entanglement and superconducting single-photon detectors to detect the photon pairs after 100 km [Zhang et al, Optics Express, April 2008]. We also demonstrated that the distributed photon pairs can still be useful for quantum key distribution and other quantum communication tasks based on their visibility and flux (2 Hz after 100 km). The experimental setup is shown in Fig. 9, while data demonstrating the two-photon interference pattern before (83.5% visibility) and after the 100-km-long spool of fiber (80.5% visibility) are shown in Fig. 10.

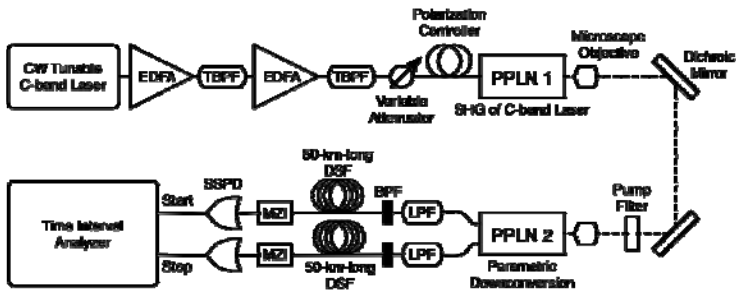


Fig. 9. Entanglement distribution. TBPF: tunable band-pass filter. PPLN1: a RPE PPLN waveguide for second harmonic generation of the pump source. PPLN2: a fiber pigtailed asymmetric Y-junction RPE PPLN waveguide for parametric down-conversion. LPF: long-pass filter to remove the 780-nm pump light and other parasitics. BPF: 0.8-nm-wide bandpass filter. SSPD: superconducting single-photon detector. TIA: time interval analyzer. Solid lines represent optical fibers and dotted lines represent free-space propagation.

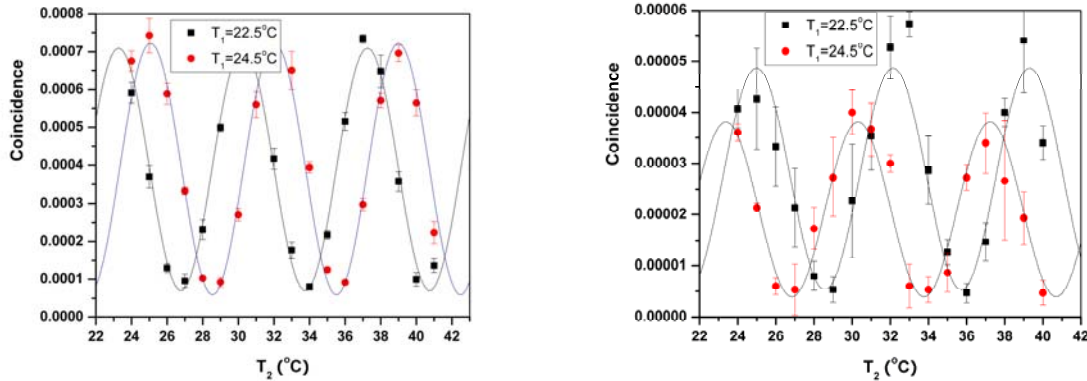


Fig. 10. Two-photon interference pattern (left) before and (right) after 100-km-long fiber; T_1 is the temperature of the PLC MZI in the signal channel, while T_2 is the temperature in the idler channel. The Y-axis represents the coincidence rate per signal photon with an average of 0.5 million signal photons.

Using the very same asymmetric Y-junction RPE PPLN waveguide device as part of a slightly different experimental setup (see Fig. 11), we further demonstrated the bunching property of parametrically generated identical photons at telecommunication wavelengths via the Hong-Ou-Mandle (HOM) dip [Zhang et al, submitted, 2008]. Here, two photons, the signal and idler photon generated inside the waveguide-based parametric downconverter, overlap at a fiber-based beam splitter from different inputs. Quantum mechanics dictates that two identical photons will bunch together upon either beam splitter output and no coincidence of the two outputs will be observed. Classical light fields also exhibit a similar destructive interference, but only with a 50% visibility. Therefore, the HOM dip is often utilized to demonstrate the difference between the regime of quantum optics and its classical counterpart. The visibility of the dip in our experiment was 80% without subtraction of any noise terms at a peak pump power of 4.4 mW (see Fig. 12). The new technology developed in the experiment can find various applications in the research field of linear optics quantum computation in fiber or quantum optical coherence tomography with near infrared photon pairs.

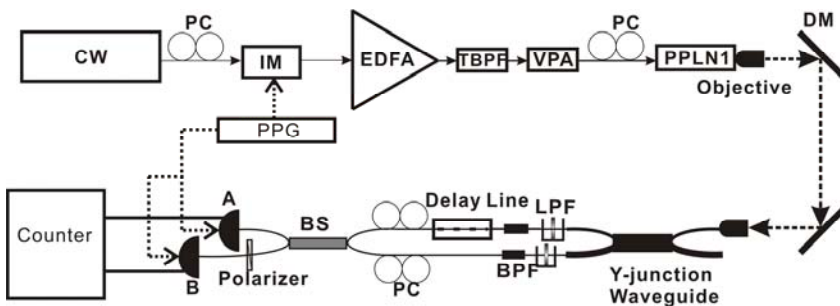


Fig. 11. Diagram of the experimental setup; IM: intensity modulator, VPA: variable power attenuator, A and B: InGaAs APDs, BS: beam splitter.

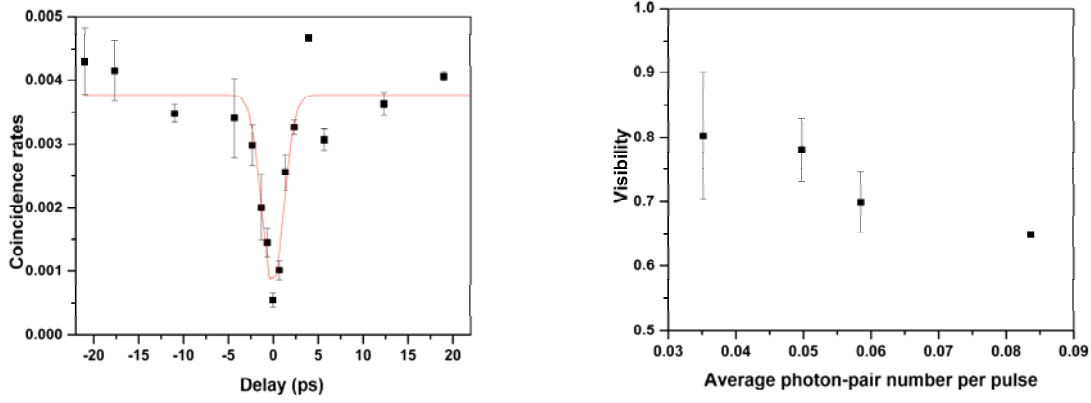


Fig. 12. (left) HOM dip. We took three sets of data for each point in the graph to estimate the measurement uncertainty. The error bars result from the data sets' standard deviation. (right) HOM dip visibility with versus average photon-pair number per pulse.

Single-photon source based on PDC in bulk materials (*Kwiat, Migdall, White*)

A deterministic single-photon source is of great value in both quantum communication experiments as well as quantum computing experiments. Our quasi-deterministic setup employs a laser that periodically sends a pulse into a storage cavity, to repeatedly pass through a crystal, giving a chance to produce a pair of photons. One of these photons is detected, and the other is then stored, to be released later at a predetermined time. As the initial pump pulse passes through the crystal in subsequent cycles, more pairs may be created, so the old photon is discarded in favor of the new one, since the most recent photon created will have the fewest cycles through the storage cavity when it is time to release it.

All of the optics for this source are in place, and all of the individual components are working properly. As shown in Fig. 13, we have successfully demonstrated pump cycling and seen downconversion events on multiple cycles, with exponentially decreasing counts as the pump cycles through many times. We have also successfully demonstrated cycling of single downconversion photons through the storage cavity, with ~96% transmission per cycle (which may be the best switchable storage cavity for single photons).

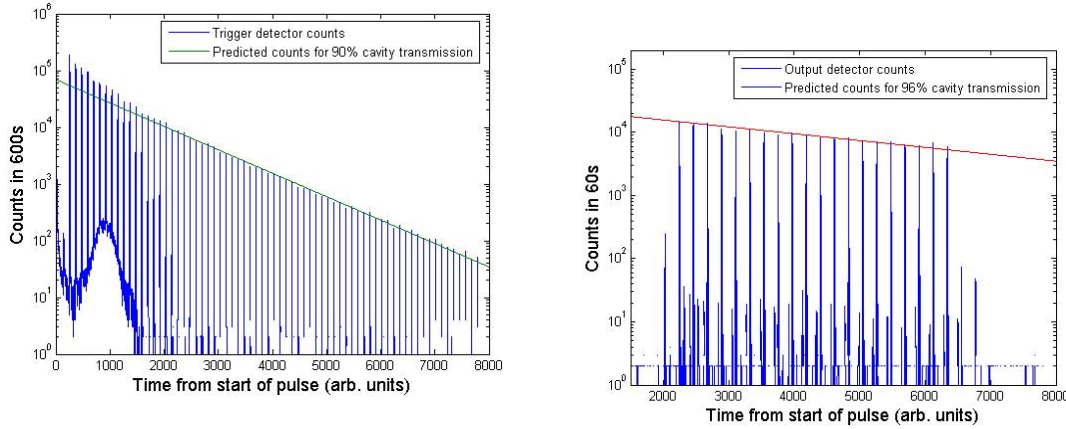


Fig. 13. Plots showing the downconversion singles counts as the pump is cycled through the UV cavity (left) and singles counts as the single photons from downconversion are cycled through the single photon storage cavity.

Efficient generation of N00N states using SPDC (*Kwiat*)

We have proposed a novel method for generating N00N states, with theoretically unit efficiency. A N00N state can be used for quantum metrology as well as for quantum lithography. We are basing the system on the fact that a N00N state in the left/right circular polarization basis can be expressed as a product state of linearly polarized photons:

$$(\hat{a}_L^\dagger)^N + (\hat{a}_R^\dagger)^N = \prod_{n=0}^{N-1} (\cos(n\pi/N) \hat{a}_H^\dagger + \sin(n\pi/N) \hat{a}_V^\dagger)$$

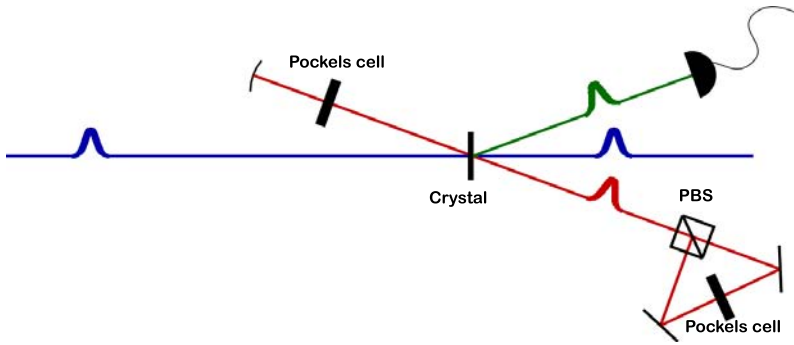


Fig. 14. Proposed setup for creating N00N states. The pulsed light emits single heralded photons one at a time into the cavity. The photons in the cavity have their polarization rotated by the top Pockels cell, and can be switched out of the cavity with the polarization-independent switch at the bottom right.

Such a state of linear photons can be built up by collecting the heralded single photons from downconversion into a polarization independent cavity (Fig. 14). Each time a photon is detected, all of the photons in the cavity are rotated by π/N by a Pockels cell. After N photons are detected, all of the photons are switched out through a polarization-independent switch. This switch can be realized with a Sagnac interferometer with a polarizing beamsplitter. A Pockels cell in the interferometer can direct the input light to either output port of the beamsplitter.

Note that this experimental setup is

similar to that of our single-photon source. Namely, we are emitting heralded single photons into a switchable storage cavity using a pulsed laser.

The practical performance is limited by many factors, mainly the imperfect transmission of the cavity and detection inefficiency. The predicted performance is shown in Fig. 15 for several different size N00N states. Notice that the probability of successfully creating the state always approaches unity as the various experimental imperfections disappear. The straight lines show the best known competing technique to realize N00N states; our method is exponentially more efficient.

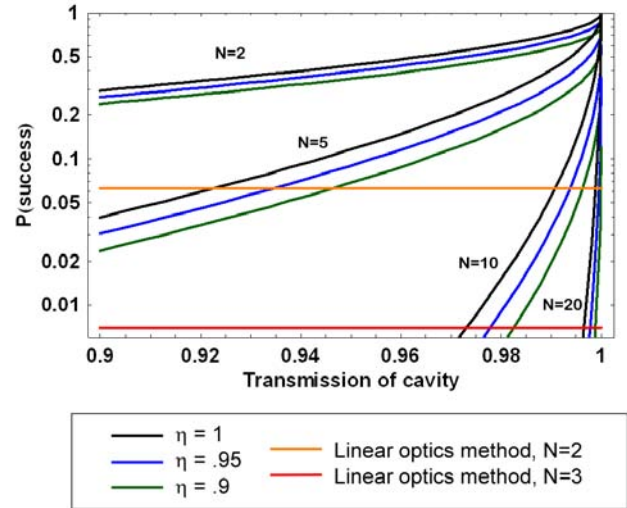


Fig. 15. Performance of our system as a function of cavity transmission and detector efficiency η .

Improving bulk downconversion entangled-photon sources (Kwiat, White)

We have successfully demonstrated a robust, high quality, large-aperture source of degenerate and non-degenerate Type-I entangled photons using BiBO, a highly nonlinear non-hygroscopic biaxial crystal, pumped with a diode laser source. Since the cw-diode laser source has a certain bandwidth, the phase ϕ in produced state $|HH\rangle + \exp(i\phi)|VV\rangle$ depends on the pump wavelength (which in the time domain leads to an effective delay between the $|HH\rangle$ and $|VV\rangle$ cones resulting in effective decoherence). We have successfully compensated for this effect in BiBO as shown in Fig. 16 by incorporating a birefringent crystal before the downconversion crystal and adding an effective delay between the two pump polarizations. The phase ϕ additionally depends on the emission directions of the downconverted photons. When collecting over large irises, one integrates over the range of ϕ , effectively decohering the state. Fig. 16(b) shows the theoretical and experimental phase gradients for nondegenerate downconversion in BiBO. The theory for biaxial crystals is nontrivial and we are currently exploring the slight discrepancy between our theory and experimental results. Fig. 17 shows our experimental and calculated results for spatial compensation in BiBO for both degenerate and non-degenerate downconversion (temporal compensation is included here). We have successfully achieved a fidelity greater than 98% (97%) for degenerate (nondegenerate) downconversion in BiBO using a diode laser source.

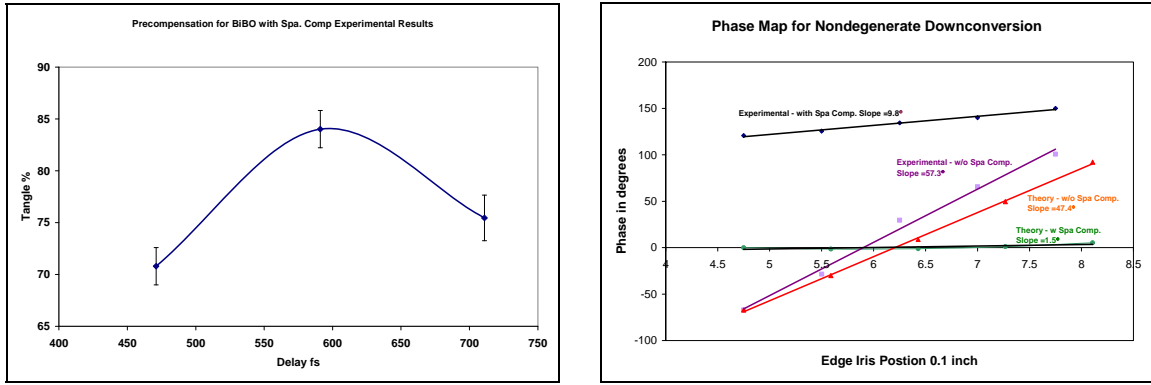


Fig. 16. a. Experimental results showing how temporal precompensation improves the entanglement quality (tangle) for Type-I entangled photons generated using BiBO, .b. Experimental data and theory curves for expected spatial phase slope for nondegenerate downconversion in BiBO.

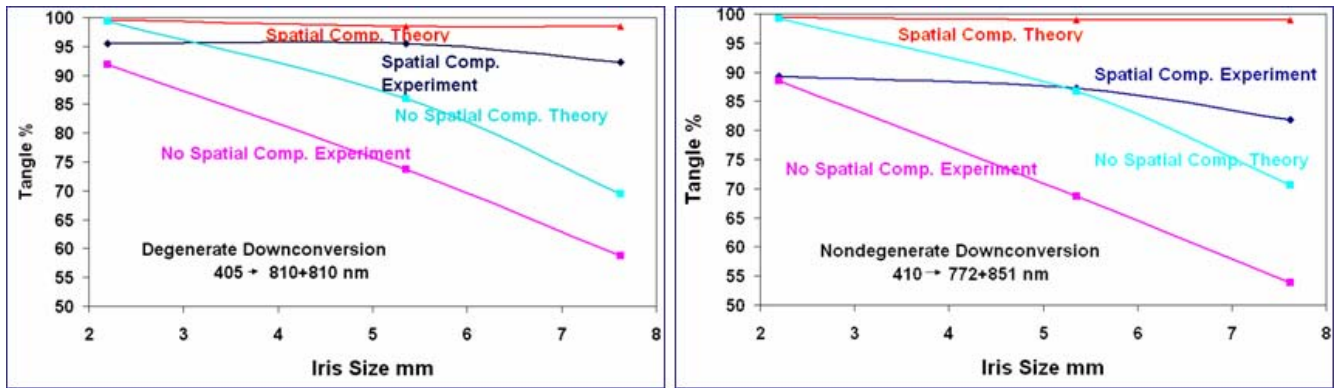


Fig. 17. Experimental and theoretical results showing how spatial compensation improves the entanglement quality (tangle) for both degenerate (left) and nondegenerate (right) Type-I entangled photons generated using BiBO.

Also, we have used our simulation code to investigate the feasibility of using a high-power light emitting diode (LED) to pump the downconversion crystals. There are two properties of LED's that can limit the entanglement of a LED-pumped source, the broad bandwidth (~ 10 nm) and the large angular divergence of the light. We have previously reported calculations that suggest the bandwidth can be precompensated in the same way as the diode laser pump, by inserting a suitable birefringent crystal in the pump beam before the downconversion crystals. The spread in pump k-vectors from the extended source LED reduces both the downconversion efficiency and quality. The efficiency is reduced due to poor phase matching in the downconversion crystals and the large angular spread of the downconversion photons. The first effect reduces the number of pump photons that are downconverted and the second effect reduces the number of downconversion photons that are collected per unit solid angle. The quality of the entanglement is reduced because the large angular spread of the downconverted photons produced a large phase gradient across the collection irises, thereby increasing the distinguishability of the photons and reducing the tangle. Using our simulation code we were able to design a precompensation crystal that would correct for phase gradients introduced by both the temporal bandwidth and the angular divergence of the pump. Encouraged by these results, we tried to observe SPDC from 20-mW, 405-nm LED's. Using simple optical elements, we were unable to suitably collimate the LED beam to produce a beam of sufficient intensity to produce a measurable downconversion signal. It may be possible to design custom optics that are able to produce a suitably bright beam but we have not pursued that avenue. Our conclusion is that it may be possible to produce an LED-pumped SPDC source but that the cost of the custom optics and necessary compensation crystals will make such a source more expensive than a laser diode-pumped source.

Optical properties of NV-centers in diamond (Lukin)

We have performed detailed studies of coherence properties associated with optical transitions of individual NV centers. Using a combination of spectral measurements of NV fluorescence, optical Rabi oscillations and spin echo we showed that optical coherence times are in the range of 10 ns, limited by spontaneous emission. In addition, we investigated optical selection rules for various NV centers, and demonstrated, for the first time, near-single-shot optical readout of NV spin states. We are presently completing the demonstration of spin-photon entanglement using this system.

We presented a theoretical analysis of the electron spin decoherence in single Nitrogen-Vacancy defects in ultra-pure diamond. The electron spin decoherence is due to the interactions with Carbon-13 nuclear spins in the diamond lattice. Our approach took advantage of the low concentration (1.1%) of Carbon-13 and their random distribution in the diamond lattice by an algorithmic aggregation of spins into small, strongly interacting groups. By making use of this disjoint cluster approach, we predicted a possibility of non-trivial electron-spin dynamics that cannot be described by a single time constant. This dependence is caused by a strong coupling between the electron and few nuclei and results, in particular, in a substantial echo signal even at microsecond time scales. Our results were in good agreement with recent experimental observations. [cond.mat.other/0805.0327, submitted to Phys. Rev. B (2008)].

We investigated the coherence properties of individual nuclear spin quantum bits in diamond when a proximal electronic spin associated with a nitrogen-vacancy (NV) center is being interrogated by optical radiation. The resulting nuclear spin dynamics are governed by a time-dependent hyperfine interaction associated with rapid electronic transitions, which can be described by a spin-fluctuator model. We showed that due to a process analogous to motional averaging in nuclear magnetic resonance, the nuclear spin coherence can be preserved after a large number of optical excitation cycles. Our theoretical analysis is in good agreement with experimental results. It indicated a novel approach that could potentially isolate the nuclear spin system completely from the electronic environment. [Phys. Rev. Lett. **100**, 073001 (2008)].

Microstructure fiber-based two-photon source (Migdall)

We previously demonstrated a microstructure fiber-based entangled photon source using a Sagnac interferometer design. While this design allows for both high and improved spectral brightness (17 kHz/ 0.15 nm at $g^{(2)}(0)=0.1$ and 0.0026 pair/pulse) and broad spectral coverage (20 nm) for the photon pairs emitted, it, like all fiber sources has been limited to less than 10% two-photon efficiency. A survey of sources over the past decade has shown that none have exceeded this level. We have focused our efforts on breaking out of this limit. By using end treatments that expand the single mode to before exiting the fiber we are able to make use of better optics. The larger mode allows off the shelf lenses with appropriate antireflection coating and the larger size allows for very mechanically stable optical coupling. We have used this advance along with an improved, more compact design to achieve extraction efficiencies of ~25% (without detector efficiencies), with further improvements planned. This higher efficiency and better stability will allow us to implement a four-photon heralded entangled pair source.

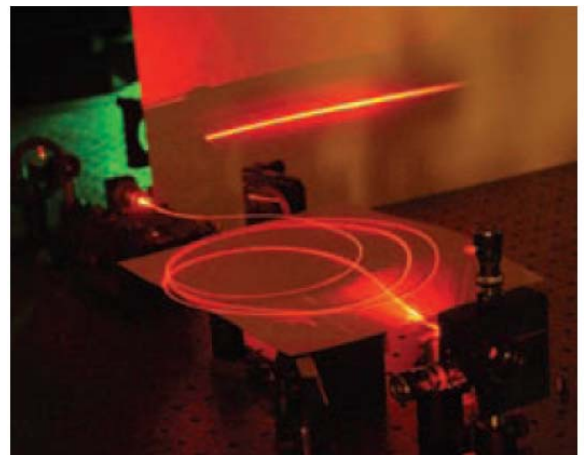


Fig. 18: Dispersed two-photon output of microstructure fiber showing broadband coverage of the source.

2. Detectors

Demonstrate high-efficiency upconversion of 1550-nm photons in bulk and waveguide geometries (Kwiat, Fejer, Yamamoto)

Waveguide geometries (Fejer)

While system experiments were underway, we designed, fabricated and started testing the first generation of short-wavelength-pump RPE PPLN waveguide-based frequency upconverters meant for single-photon detection at telecommunication wavelengths. These devices can be used to either upconvert photons at ~ 1550 nm or ~ 1064 nm to the near-infrared, depending on the choice of pump wavelength; 1550 nm for detection at 1064 nm, and vice versa. The purpose of these devices is twofold as well. They will aid a better understanding of the parametric noise sources encountered in upconversion-based single-photon detectors, as well as serve as fast low-noise single-photon detectors at wavelengths between 1050 – 1100 nm, a range not readily accessible with commercial detectors.

The previously mentioned study of the upconversion-based single-photon detector's noise performance requires further requires a frequency-agile narrow-linewidth infrared pump source which can cover a broad wavelength range around 1800 nm. Measuring the detector's dark-count rate (DCR) as a function of pump wavelength will allow us to validate our theoretical model based on spontaneous Raman scattering, which predicts that the DCR can be reduced by more than two orders of magnitude when the pump is at a longer wavelength than the signal. Recent experimental results from researchers at NTT are highly encouraging [Kamada et al, Optics Letters, 2008]. We previously described the concept of a monolithic ring optical parametric oscillator (OPO) based on bulk PPLN. In such a device, the end facets are polished and coated to facilitate resonating the signal while passing the pump and idler waves (see Fig. 19). When pumped with a narrow-linewidth CW laser at 1064 nm, such a device can generate a tunable signal at 1800 nm, with the corresponding idler at 2600 nm. The first generation of these devices has already been designed and fabricated, and is currently being tested in our lab. Initial experimental results led us to look into mid-infrared absorption mechanisms in magnesium-doped lithium niobate and stoichiometric lithium tantalate, which cause a significant increase in the OPO's oscillation threshold.

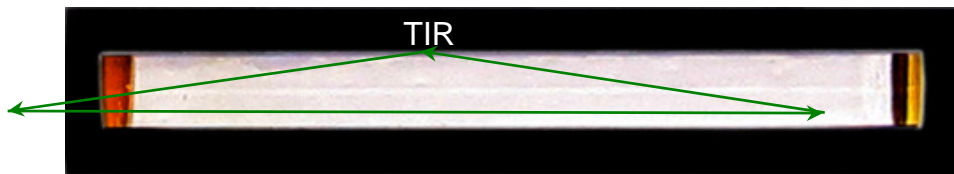


Fig. 19. Photograph of a monolithic bulk PPLN optical parametric oscillator used for generation of long-wavelength mid-infrared radiation. Notice the curved end facets serving as integrated mirrors for the resonant signal. The end facets are coated for the resonant signal (HR), as well as the idler and pump (AR). The green triangle inscribed inside the chip represents the signal path including a total internal reflection (TIR) bounce at the top facet of the device.

Superconducting bolometric single-photon detectors (Eckstein)

During the past year we redesigned the device layout and processing recipes to include lithographic shunt resistors. These were included to carry the current when the current-driven link goes normal and allow the niobium link to reset back to the superconducting state. We have studied light detection using a range of shunt resistance values, from 1 to 150 Ohms, in ten measurable samples. Devices were tested for low-frequency response using the setup we put together earlier – a chopped laser source coupled to the link via a fiber and then signal detection using a lock-in amplifier. Devices incorporating lower resistance shunts were linear in incident power and gave similar photon detection signal levels as externally shunted devices did last year. Devices were also tested at higher frequency using a 1 GHz digitizing oscilloscope. We found that wafers having large shunt resistance values were always hysteretic. For shunt values under several Ohms, we did not see hysteresis, but the fast time scale signal level was too small to be detected. The problem appears to be not so much with the

device as with the testing setup, so it is something we should be able to fix. The noise level we measure with large bandwidth detection is very large, about 10^3 times Johnson noise, given the specific shunt value.

Upgrade Solid-State Photomultipliers (SSPM) and Visible-Light Photon Counting (VLPC) Detectors (Kwiat)

With low-noise electronics, noise-shielding and stable cryogenic operation in place, we started performing detector-efficiency measurements. Fig. 20a shows the overall (source-to-detector) efficiency at 635 nm at several different bias values. The maximum overall efficiency is 56%, corresponding to an inferred intrinsic peak efficiency of $88\pm 8\%$. However, for these measurements, the coupling optics are not optimized. By incorporating our optimized detectors and coupling optics, we anticipate actual detection efficiencies in excess of 90%. We had previously deposited anti-reflection coatings on the VLPCs to overcome the $\sim 25\%$ reflection loss using in-house fabrication facilities. We observed that these coatings were sensitive to repeated thermal-cycling and had identified and tested coatings (from a commercial vendor, INO in Canada) that are capable of withstanding repeated cryogenic conditions. However, due to massive equipment failure, INO cannot meet our needs any longer and we are currently looking for other companies capable of depositing high-quality cryogenic coatings. Also, we have successfully observed multi-photon detection using a fast oscilloscope (Fig. 20b). We have built a custom ultra-fast four-channel analyzer (FCA) capable of performing pulse-height analysis measurements on the fast VLPC output pulses. We are currently working on the software to control the FCA and to provide user-friendly readout; this should be completed shortly.

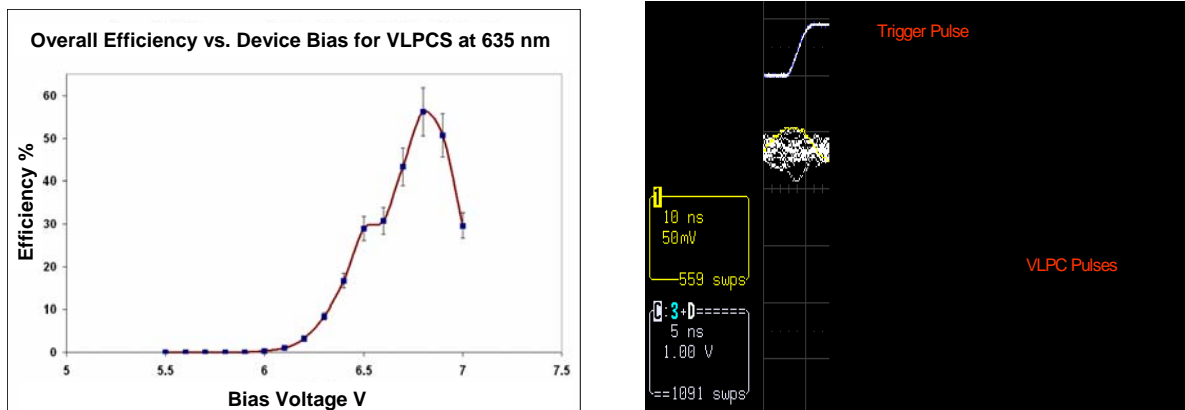


Fig. 20. a. Overall efficiency of VLPCs vs. bias voltage at 8K. b. Scope trace of detector output pulses. The quantized pulse heights indicate photon-number resolution.

Photon-counting detector metrology (Migdall)

After publishing the results of our high accuracy metrological verification of the two-photon method for calibrating photon counting detection efficiency (Fig. 21) we moved forward with our plan for disseminating this higher accuracy photon counting to the user community. To do this we procured 10 units of a high-gain low-noise visible detector amplifier that we designed specifically for simple calibrations of photon-counting detectors (Fig. 22). The units are designed to operate with high accuracy at the low light levels that are required to avoid saturation of the photon counting detectors to be calibrated. The design uses a detector with high spatial response uniformity ($\sim 0.1\%$). In addition, the photodiode is in a thermoelectrically cooled housing to allow operation at high shunt resistances ($\sim 5G\Omega$). This high shunt resistance in turn allows high feedback resistors and high gain, while keeping the system noise low enough to achieve the desired 0.5% (or better) uncertainty. The 10 units have been delivered and are currently undergoing tests to verify proper operation such as long term stability. Once they have been determined to operate properly they will be calibrated at NIST's spectral calibration facility. Once completed, they will be available for loan to team members and others. This provides a guide to others on how to use this method with high accuracy and confidence. Results of this work will be presented at NEWRAD Oct. 2008.

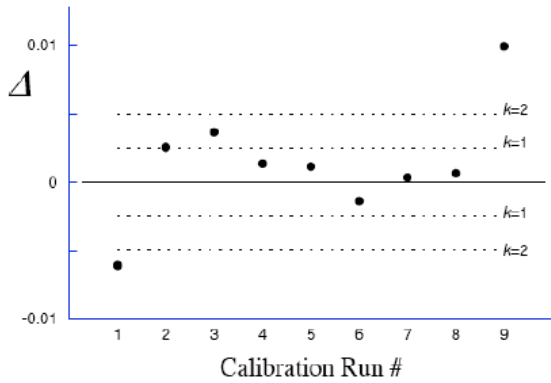


Fig. 21. Comparison between two absolute calibration methods: correlated photon pair and substitution (traceable to NIST scale). The size of the confidence bands reflects the uncertainty of each individual comparison and indicates the consistency of the overall comparison with zero bias between the two methods.



Fig. 22. One of ten high-gain low-noise Si detector/amplifier units to be used to transfer calibrations to photon-counting detectors.

Multiplexed detector scheme for high photon counting rates (Migdall)

We have implemented an improved control circuit for our scheme to reduce effective photon-counting detector deadtime using multiplexed detection scheme with InGaAs detectors. This system used two InGaAs detectors which are normally operated with a 10 microsecond deadtime (Fig. 22). We previously used the setup to corroborate our theory showing that one can achieve higher photon counting rates with this multiplexed system than is otherwise possible with individual detectors. In the recent improvement we dealt with the issue of deadtime associated with the trigger-control electronics, and demonstrated an additional improvement (over our previous result) of more than a factor of 2 in the operating count rate while maintaining the same 10% deadtime fraction.

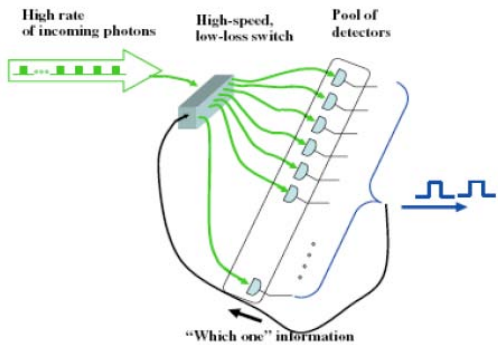


Fig. 22. A pool of detectors and a fast switch are used to register a high rate of incoming photons. Incoming photons are switched to a ready detector. If it fires, the detector is switched out of the ready pool until recovery. If it does not fire, that detector remains ready.

3. Photon storage

Using an asymmetric storage-cavity scheme for photon memory (Kwiat)

We have devised a configuration for a digital delay line that should allow us to store a photon from 13 ns to 13.0 μ s, in 13 ns increments (chosen somewhat arbitrarily, to correspond to the period of a typical mode-locked Ti:Saph laser), using three cavities, while maintaining the spatial mode throughout. The first cavity has a path length of 13 ns, the second a path length of 130 ns, and the third a path length of 1.30 μ s. A light pulse can pass through each cavity up to nine times, controlled by an optical switch (a Pockels cell) in the cavity. The 1.30- μ s cavity is made with two cylindrical mirrors axially rotated with respect to one another. Assuming 99.99% mirror reflectivity and 98% transmission through the switching elements, we predict the performance shown in Fig. 23. The previous mirror used for the long cavity had an unexpectedly low reflectivity of 99.83%; we have thus obtained a new one. Preliminary measurements indicate a reflectivity $>99.93\%$, but we are still verifying the uncertainty in that measurement.

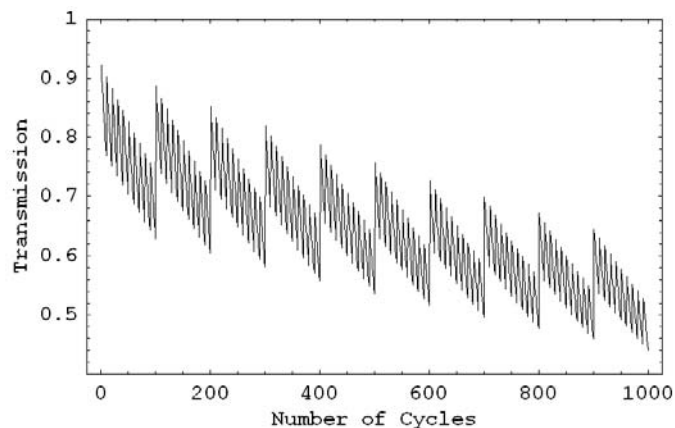


Fig. 23. The transmission of the delay line as a function of the number of cycles (each cycle is 13-ns long). The “sawtooth” behavior arises from the fact that whenever the photon is switched from going through one cavity nine times to the next cavity once, there is a jump in transmission.

4. System-level applications

New protocols for long-distance quantum communication and schemes for quantum computing (Lukin)

Reliable preparation of entanglement between distant systems is an outstanding problem in quantum information science and quantum communication. In practice, this has to be accomplished by noisy channels (such as optical fibers) that generally result in exponential attenuation of quantum signals at large distances. A special class of quantum error correction protocols, quantum repeater protocols, can be used to overcome such losses. In this work, we introduced a method for systematically optimizing existing protocols and developing more efficient protocols. Our approach made use of a dynamic programming-based searching algorithm, the complexity of which scales only polynomially with the communication distance, letting us efficiently determine near-optimal solutions. We found significant improvements in both the speed and the final-state fidelity for preparing long-distance entangled states. [PNAS 104, 17291 (2007)].

We described and analyzed an efficient register-based hybrid quantum computation scheme. Our scheme is based on a probabilistic, heralded optical connection among local five-qubit quantum registers. We assumed high-fidelity local unitary operations within each register, but the error probability for initialization, measurement, and entanglement generation can be very high ($\sim 5\%$). We demonstrated that with a reasonable time overhead our scheme can achieve deterministic nonlocal coupling gates between arbitrary two registers with very high fidelity, limited only by the imperfections from the local unitary operation. We estimated the

clock cycle and the effective error probability for implementation of quantum registers with ion traps or nitrogen-vacancy centers. Our scheme capitalized on an efficient two-level pumping scheme that in principle can create Bell pairs with arbitrarily high fidelity. We introduced a Markov chain model to study the stochastic process of entanglement pumping and map it onto a deterministic process. Finally we discussed requirements for achieving fault-tolerant operation with our register-based hybrid scheme and also presented an alternative approach to fault-tolerant preparation of Greenberger-Horne-Zeilinger states. [Phys. Rev. A 76, 062323 (2007)].

Quantum information encoding into transverse spatial modes (*Kwiat, White*)

Previously we reported the use of our source of pairs of photons hyper-entangled in polarization and orbital angular momentum (OAM) to achieve high-quality, complete and deterministic Bell-state analysis with linear-optics. After implementing several modifications to the system, we have been able to improve our results somewhat, so that now we can determine the encoded Bell state with an average success probability of 95%, with a reduced uncertainty.

Our other main effort has involved using the hyperentanglement-enabled Bell-state analysis to realize full Direct Characterization of Quantum Dynamics (DCQD). We have identified all processes that will be used in our demonstration of DCQD. The processes include the identity, unitary rotations (trivial and non-trivial), partial polarizer, and some depolarizer channels (using rapidly changing liquid crystals). Given that our setup couples the photons into optical fibers for mode filtering, every component inserted in the path shouldn't noticeably deviate the beam. For a quick characterization of the different processes, we have identified and acquired components with that property. This avoids going through the time-consuming alignment procedure every time we place a new component/process. In order to compare DCQD with standard quantum process tomography, we have thus far performed the standard reconstruction of all processes and achieved a process fidelity with the ideal of 99% on average.

DCQD uses a set of input states with two free parameters. We have become aware that the achieved process fidelity depends on the particular value of these parameters. The analytical solution performs well for most processes, but ultimately adaptive techniques will be required. In addition, in collaboration with M. Mohseni, we have extended the original proposal to incorporate errors in the preparation of the input states and the Bell-state analysis. Some errors can be easily factorized and easily fed into the reconstruction (such as white noise in the input states), while others require a process tomography of the input states and Bell-state analysis. This last step is, basically, the process tomography of the identity. We estimated the quality of the future DCQD reconstructions by performing preliminary measurements of the diagonal element of the identity process. We achieved low reconstruction errors, from 1% to 3%. We can use this information to factor out errors in the reconstruction; however, we still need to investigate how to decouple errors in the input states from those in the measurement.

Quantum networks on chip (*Vuckovic*)

To overcome the problems of QD inhomogeneous broadening and their spectral misalignment from cavity resonances, as well as the fabrication imperfection of photonic crystals, we have developed methods for local, reversible tuning of a quantum dots on a photonic crystal chip [Faraon et al., Applied Physics Letters, 2007], and for selective tuning of cavity resonances [Faraon et al., Applied Physics Letters, 2008]. The first method is based on laser-induced local heating (a below-GaAs bandgap laser is used to heat a Cr/Au pad next to the GaAs cavity – see Fig. 24a - without exciting photoluminescence in the sample) and can be used to shift the QD wavelength by up to 1.8nm. A second method is based on overcoating of photonic crystals with chalcogenide glasses and their subsequent photodarkening with a laser, and can be used to tune cavity resonances by several nm without Q-degradation (Fig. 24 e-f). Our experimental results for both methods are shown in Fig. JV4, and they have or are being employed in our cavity QED experiments, as well as in the integrated cavity-waveguide configuration (see Fig. 25 – [Faraon et al., Opt. Exp., 2008]).

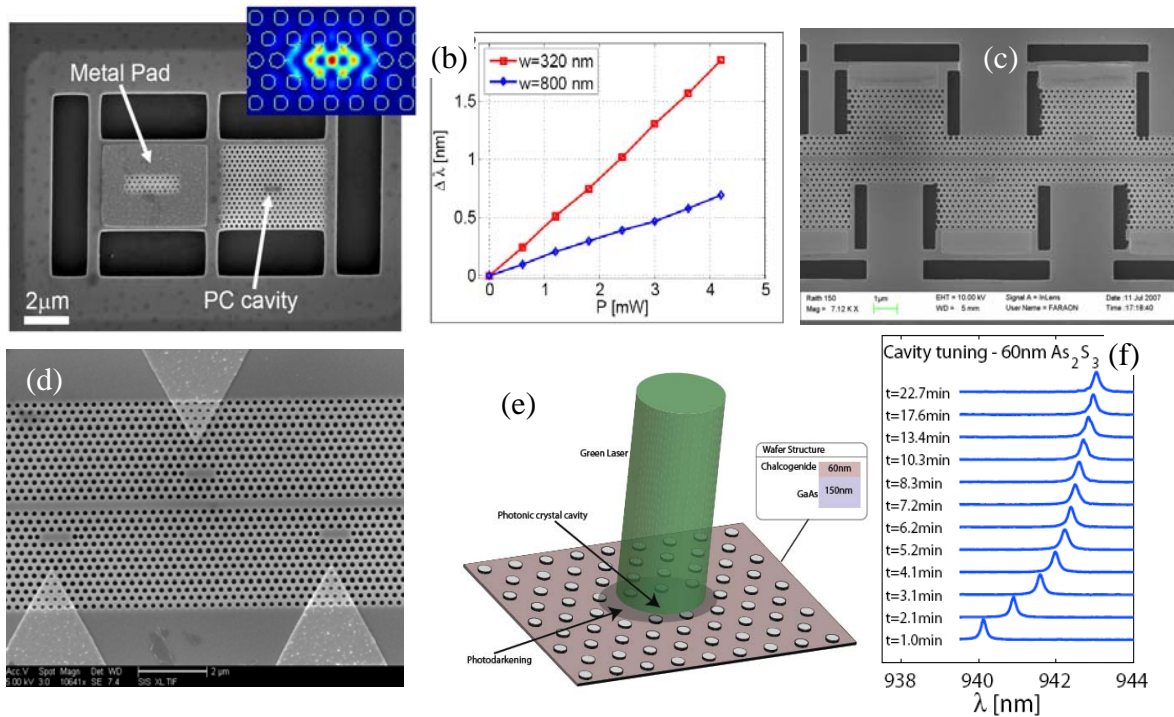


Fig. 24: (a) Fabricated structure for laser-induced selective tuning of a quantum dot in a photonic crystal cavity by local heating. The device consists of a photonic crystal cavity with embedded quantum dot and heating pad next to them. The heating pad is made of a thin layer of Cr/Au deposited on GaAs, and structure is tuned by illumination with a 960nm CW laser (below the band gap of GaAs, so that background photoluminescence is not induced). (b) Selective tuning of a single InAs/GaAs quantum dot by this technique, by up to 1.8nm. (c),(d) Extensions of the local tuning technique, enabling selective tuning of quantum dots in coupled cavity-waveguide structures. (e) Method for local PC-cavity tuning by photodarkening a thin chalcogenide layer on top of it. (f) Spectra showing the tuning of the photonic crystal cavity with chalcogenide nanomembrane layer on top of it.

We have also demonstrated dipole-induced transparency in integrated cavity-waveguide configuration – see Fig. 25 [Faraon et al, Optics Express, 2008]. Basically, we have coherently probed a QD embedded in a photonic crystal cavity via a laser beam injected to the cavity using a photonic crystal waveguide. The outcoupling from the waveguide was achieved using a grating coupler, as shown in Fig. 25.

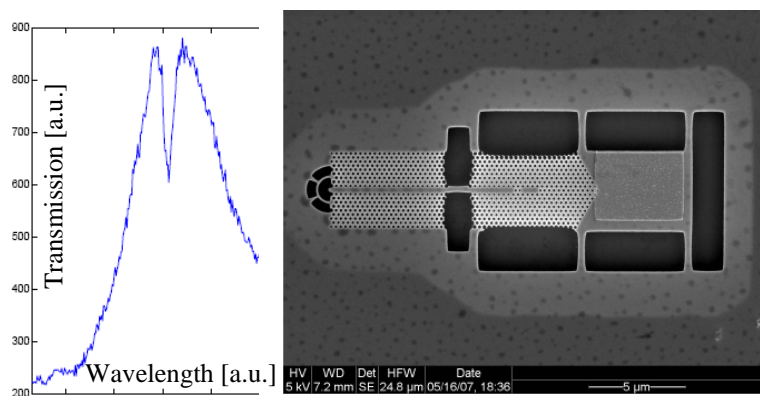


Fig. 25. Normalized transmission (left) through a waveguide-coupled photonic crystal cavity (right). When a quantum dot is tuned onto the cavity resonance, a dip in the cavity transmission appears.

Differential phase shift quantum key distribution (Yamamoto)

We have implemented a 10 GHz clock frequency BBM92 QKD system using a PPLN waveguide down-converter and SSPDs. A secure key was created over 100 Km optical fiber.